© 2014. Published by The Company of Biologists Ltd | The Journal of Experimental Biology (2014) 217, 4018-4028 doi:10.1242/jeb.107656

RESEARCH ARTICLE

Musculoskeletal modelling deconstructs the paradoxical effects of elastic ankle exoskeletons on plantar-flexor mechanics and energetics during hopping

Dominic James Farris[1,2,*], Jennifer L. Hicks[3], Scott L. Delp[3,4] and Gregory S. Sawicki[2]

ABSTRACT

Experiments have shown that elastic ankle exoskeletons can be used to reduce ankle joint and plantar-flexor muscle loading when hopping in place and, in turn, reduce metabolic energy consumption. However, recent experimental work has shown that such exoskeletons cause less favourable soleus (SO) muscle–tendon mechanics than is observed during normal hopping, which might limit the capacity of the exoskeleton to reduce energy consumption. To directly link plantar-flexor mechanics and energy consumption when hopping in exoskeletons, we used a musculoskeletal model of the human leg and a model of muscle energetics in simulations of muscle–tendon dynamics during hopping with and without elastic ankle exoskeletons. Simulations were driven by experimental electromyograms, joint kinematics and exoskeleton torque taken from previously published data. The data were from seven males who hopped at 2.5 Hz with and without elastic ankle exoskeletons. The energetics model showed that the total rate of metabolic energy consumption by ankle muscles was not significantly reduced by an ankle exoskeleton. This was despite large reductions in plantar-flexor force production (40–50%). The lack of larger metabolic reductions with exoskeletons was attributed to increases in plantar-flexor muscle fibre velocities and a shift to less favourable muscle fibre lengths during active force production. This limited the capacity for plantar-flexors to reduce activation and energy consumption when hopping with exoskeleton assistance.

KEY WORDS: Assistive robotics, Dynamics simulation, Energetics, Locomotion, Metabolic energy, Muscle mechanics

INTRODUCTION

Recent advances in exoskeletons or wearable robotic technology designed to assist human locomotion frequently include passive spring-loaded elements to conservatively store and return energy (Ferris et al., 2006; Grabowski and Herr, 2009; Wiggin et al., 2011; Bregman et al., 2012; Farris and Sawicki, 2012a). The use of springs takes inspiration from the actions of series elastic components (SECs) in muscle–tendon units (MTU) of the leg (Cavagna, 1977; Alexander, 1988; Fukunaga et al., 2001; Lichtwark and Wilson, 2006). During locomotion, energy is stored in the SECs of anti-gravity muscles during the first half of stance as the body centre of mass (COM) either passes over (walking) or compresses (running) the support leg. This energy can then be returned later in stance to help propel the COM into the next step. This spring-like action of the leg has inspired wearable technologies or exoskeletons that attach externally to the leg and aim to provide parallel assistance to the underlying muscles. This usually has the aims of lowering metabolic energy consumption, unloading biological tissues and/or providing mechanical power that muscles cannot. Grabowski and Herr (Grabowski and Herr, 2009) have shown previously that the metabolic cost of hopping in place could be reduced by an exoskeleton that employed a leaf-spring in parallel with the whole leg. The participants in their study reduced the contribution of biological tissues to leg stiffness and effectively shared the load with the exoskeleton. The plantar-flexor muscle group makes excellent use of elastic mechanisms, storing and returning energy in the compliant Achilles tendon during walking and running (Ishikawa et al., 2005; Lichtwark et al., 2007; Farris and Sawicki, 2012b). This has inspired the design of ankle exoskeletons that store and return energy in a spring that is placed in parallel with the plantar-flexors, attached to the body via an ankle-foot orthosis (Ferris et al., 2006; Wiggin et al., 2011; Farris and Sawicki, 2012a). These exoskeletons are intended to reduce the mechanical demand on the plantar-flexors and consequently, reduce the metabolic cost of human movement. Previous work has shown that participants hopping in such devices reduce the activation to their plantar flexor muscles and, in turn, the contribution of these muscles to ankle joint stiffness (Ferris et al., 2006).

In a recent experimental study, we showed that such exoskeletons reduce the whole-body net metabolic cost of bilateral hopping (Farris and Sawicki, 2012a). This reduction in net metabolic cost was associated with significant reductions in ankle joint work and moments (Farris and Sawicki, 2012a). In a further study, to examine mechanics of the MTU, we also employed ultrasound imaging of soleus muscle fascicles (Farris et al., 2013). These data revealed that the exoskeletons did not reduce soleus fascicle work, despite reducing muscle force and electromyographic activity. This was owing to increased soleus fascicle length change when hopping in exoskeletons. From this, we postulated that observed reductions in metabolic cost with exoskeletons were partially the result of reduced soleus muscle forces and that the mechanical work done by fascicles was less important energetically. However, our capacity to draw such conclusions was limited because our metabolic measure was whole-body net metabolic power, encompassing energy consumed by all the muscles involved in the movement, not just soleus. The ability to more directly link individual muscle mechanics and energetics would provide better insights into how spring-loaded exoskeletons affect underlying muscle function and energy consumption. This is an important step in understanding how exoskeletal devices provide assistance to the biological system.

[1]School of Human Movement Studies, University of Queensland, St Lucia, QLD 4072, Australia. [2]Joint Department of Biomedical Engineering, University of North Carolina-Chapel Hill and North Carolina State University, Raleigh, NC 27606, USA. [3]Department of Bioengineering, Stanford University, Stanford, CA 94305-4125, USA. [4]Department of Mechanical Engineering, Stanford University, Stanford, CA 94305-3030, USA.

*Author for correspondence (d.farris@uq.edu.au)

Received 4 May 2014; Accepted 24 September 2014

The Journal of Experimental Biology

The Journal of Experimental Biology (2014) doi:10.1242/jeb.107656

Ultrasound imaging of fascicles for all the relevant muscles is impracticable because of the requirement for multiple synchronised ultrasound transducers and an exoskeleton to be attached to the leg. It is also not plausible to directly measure individual muscle forces in human subjects. A viable alternative for obtaining individual muscle mechanics was to use a musculoskeletal model based on some experimental inputs (e.g. Delp et al., 1990; Zajac et al., 2003; Arnold and Delp, 2011). With knowledge of individual muscle mechanics, the metabolic energy consumed by individual muscles may be estimated using an energetics model (e.g. Lichtwark and Wilson, 2005a; Umberger and Rubenson, 2011).

In this study, we sought to better understand how spring-loaded ankle exoskeletons affect plantar-flexor muscle mechanics and energetics. To achieve this, we employed two models: (1) a musculoskeletal model to predict muscle–tendon dynamics during bilateral hopping with and without spring-loaded ankle exoskeletons and (2) an energetics model to predict the metabolic energy consumed by the muscles in the musculoskeletal model. Previously published experimental data – including electromyograms (soleus, medial and lateral gastrocnemius and tibialis anterior), kinematics and external forces (Farris and Sawicki, 2012a; Farris et al., 2013) – were used to drive simulations of muscle–tendon dynamics for seven models, each scaled to the anthropometrics of each individual experimental participant. Simulations of hopping with and without ankle exoskeletons were generated. These simulations output muscle–tendon dynamics for the medial gastrocnemius (MG), lateral gastrocnemius (LG), soleus (SO) and tibialis anterior (TA), which were passed to a previously published model of muscle energetics (Lichtwark and Wilson, 2005a) to compute individual muscle metabolic energy consumption. We hypothesised from previous experimental data (Farris et al., 2013) that plantar-flexor muscle forces would be reduced by exoskeletons but contractile work done by these muscles would be unchanged. We reasoned that plantar-flexor energy consumption would be less with exoskeletons owing to lower muscle forces and reduced muscle activation outweighing any competing effects of increased contractile element length change or velocity on muscle energy consumption.

RESULTS

Musculoskeletal model evaluation

Performance of the musculoskeletal model was primarily evaluated by comparing net ankle joint moments and powers generated by the muscles in the simulation of muscle–tendon dynamics against those calculated from an inverse dynamics solution. Fig. 1 shows the time course of instantaneous moments and powers from both solutions. For a more detailed comparison, Table 2 compares the timings and magnitudes of peak moments and powers. Generally, mean values for timings and magnitudes from the simulations of muscle–tendon dynamics were within one standard deviation of the mean values from the corresponding inverse solutions. The exception to this was that peak moments from the simulations of hopping with exoskeletons fell below this range. However, there were no statistically significant (Student's paired *t*-test, α=0.05) differences observed between simulations of muscle–tendon dynamics and inverse solutions, for any of the timing or magnitude metrics.

We also compared muscle mechanics data output from the musculoskeletal simulations with previous experimental data (Farris and Sawicki, 2012a; Farris et al., 2013). Experimental electromyography (EMG) signals were used as inputs to the model of activation dynamics. Consequently, the activations produced by this part of the model were essentially constrained to follow closely

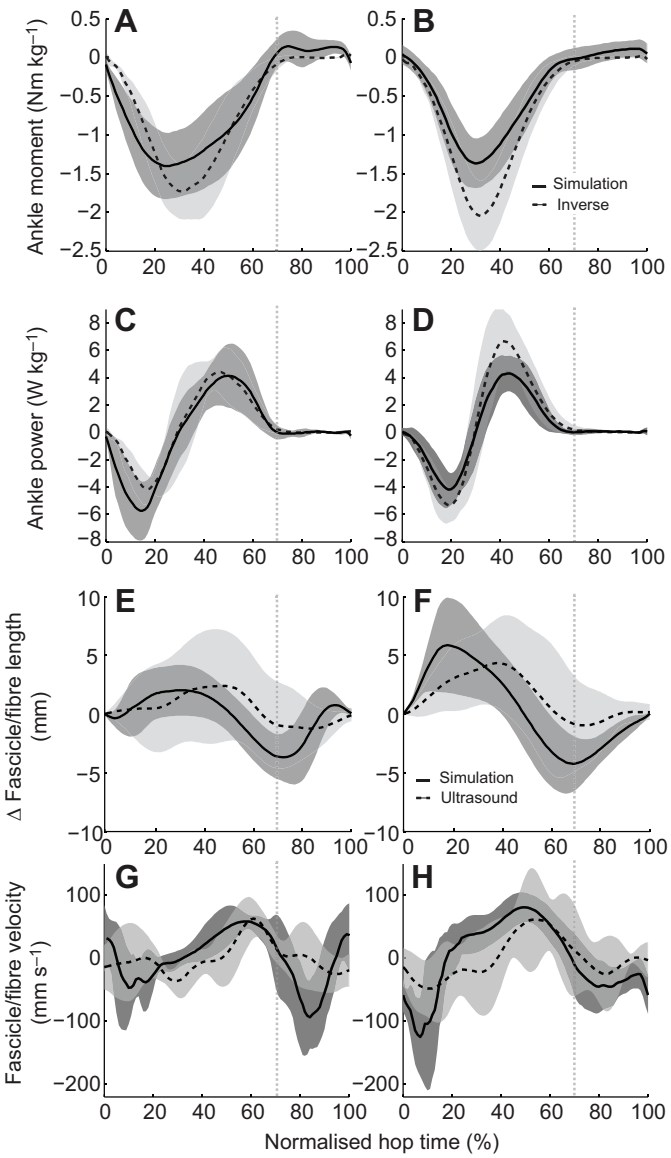

Fig. 1. Data used in the evaluation of the musculoskeletal model. A comparison of the (A,B) net ankle moments and (C,D) powers calculated from the moments produced by the muscle forces in the simulations of muscle–tendon dynamics (solid lines) and the net moments and powers calculated using an inverse dynamics approach (dashed lines). (E–H) Comparison of SO fibre length changes and corresponding velocities from the simulations with previously published (Farris et al., 2013) SO fascicle length changes and velocities measured experimentally from ultrasound imaging. The no exoskeleton condition data are shown in the left panels (A,C,E,G) and the spring-loaded exoskeleton data in the right panels (B,D,F,H). Data are the average of all seven scaled models ± s.d. (shaded regions) normalised to hop time as a percentage of the hop cycle starting from landing. The vertical dotted lines indicate take-off.

the experimental EMG data. Therefore, in the simulations, wearing exoskeletons reduced SO average activation but did not change MG and LG activation, as was shown previously using the experimental EMG (Farris and Sawicki, 2012a). Simulated SO fibre length change patterns agreed with experimental SO fascicle length change data, both showing initial lengthening upon ground contact followed by shortening, and both showing a significantly greater length change with exoskeletons (Fig. 1E,F). The magnitudes of fibre shortening during ground contact were also comparable between

The Journal of Experimental Biology (2014) doi:10.1242/jeb.107656

Table 1. Group mean (±s.d.) metrics of muscle mechanics for hopping with (SE) and without (NE) spring-loaded exoskeletons output by the simulations of muscle–tendon dynamics

	M. gastrocnemius		L. gastrocnemius		Soleus		Tibialis anterior	
	NE	SE	NE	SE	NE	SE	NE	SE
Normalised peak activation	0.79±0.14	0.86±0.13	0.84±0.16	0.81±0.11	0.76±0.09	0.69±0.19	0.60±0.17	0.73±0.14
Normalised average activation‡	0.61±0.14	0.60±0.11	0.60±0.14	0.53±0.11	0.56±0.06	0.44±0.12*	0.39±0.13	0.50±0.11
Peak fascicle shortening velocity‡ (L_0 s^{-1})	1.5±0.8	1.8±0.6	1.7±0.5	2.0±0.7	1.4±0.5	2.0±0.6*	1.3±1.1	1.6±1.3
Average fibre velocity‡ (L_0 s^{-1})	0.02±0.02	0.05±0.02*	0.04±0.03	0.06±0.02	0.01±0.01	0.03±0.02*	−0.01±0.07	−0.02±0.06
Average fibre length‡ (L/L_0)	0.81±0.16	0.64±0.09*	0.87±0.16	0.72±0.08	0.96±0.13	0.80±0.04*	0.86±0.10	0.91±0.07
Peak force (F/F_{max})	0.64±0.19	0.48±0.10*	0.59±0.20	0.38±0.15*	0.73±0.16	0.44±0.17*	0.54±0.14	0.68±0.18
Average force‡ (F/F_{max})	0.46±0.16	0.27±0.05*	0.38±0.14	0.24±0.06*	0.50±0.12	0.22±0.08*	0.30±0.14	0.39±0.15
Index of force-producing ability (F_{ind})	0.74±0.18	0.46±0.07*	0.63±0.17	0.45±0.07*	0.89±0.14	0.50±0.15**	0.79±0.27	0.77±0.20
Positive fibre work (J kg^{-1} hop^{-1})	0.063±0.02	0.040±0.01	0.031±0.01	0.053±0.02	0.032±0.01	0.036±0.02	0.040±0.04	0.048±0.03
Negative fibre work (J kg^{-1} hop^{-1})	−0.048±0.02	−0.019±0.01*	−0.016±0.01	−0.021±0.01	−0.028±0.03	−0.010±0.01*	−0.096±0.05	−0.126±0.01
Net fibre work (J kg^{-1} hop^{-1})	0.015±0.02	0.021±0.01	0.015±0.00	0.032±0.01*	0.004±0.04	0.026±0.02*	−0.056±0.05	−0.078±0.01
Positive MTU work (J kg^{-1} hop^{-1})	0.098±0.03	0.075±0.02	0.041±0.01	0.031±0.01	0.279±0.06	0.167±0.05*	0.072±0.04	0.091±0.04
Negative MTU work (J kg^{-1} hop^{-1})	−0.083±0.02	−0.056±0.02*	−0.026±0.01	−0.015±0.01	−0.276±0.07	−0.141±0.04*	−0.124±0.06	−0.056±0.02
Net MTU work (J kg^{-1} hop^{-1})	0.014±0.02	0.019±0.01	0.015±0.00	0.015±0.01	0.004±0.04	0.026±0.04*	−0.052±0.05	0.019±0.01
Ratio of fascicle to MTU positive work	0.65±0.20	0.53±0.10	1.76±0.70	1.76±0.41	0.12±0.04	0.22±0.06*	0.46±0.21	0.52±0.14
Energy consumption (J kg^{-1} hop^{-1})	0.18±0.03	0.11±0.01*	0.09±0.01	0.07±0.01	0.29±0.03	0.24±0.02	0.12±0.04	0.15±0.03

‡These variables were calculated for a period of ±25% the hop cycle either side of peak fascicle force. *Statistically significant difference between with and without exoskeletons (P<0.05). **Statistically significant difference between with and without exoskeletons (P<0.01). F, fibre force; F_{ind}, the index of force-producing capability of a muscle; F_{max}, muscle maximum isometric force; L, fibre length; L_0, optimum muscle fibre length; MTU, muscle–tendon unit.

experimental (no exoskeleton ~3–4 mm, spring-loaded exoskeleton ~5–6 mm) and simulation (no exoskeleton ~4–5 mm, spring-loaded exoskeleton ~7–8 mm) results, although slightly greater in the simulations. However, the model results showed a reduced average SO fibre length (−7 mm) with exoskeletons (Table 1), but the experimental data did not (Farris et al., 2013).

Muscle energetics

Energetics

Results from the simulations of muscle–tendon dynamics and the energetics model showed that the total rate of metabolic energy consumption for all muscles was not significantly reduced for hopping with exoskeletons (0.68±0.07 versus 0.57±0.04 J kg^{-1} hop^{-1}; ±s.d.), despite a trend for a small reduction (Table 1). Examination of individual muscles revealed that MG was the only muscle to exhibit a significant reduction in the rate of metabolic energy consumption (Table 1). Although LG and SO trended toward a reduced metabolic cost with exoskeletons, no statistically significant difference was found, and the energy consumption of TA was slightly but non-significantly greater with exoskeletons.

Muscle mechanics

Medial gastrocnemius

Simulation results showed that MG forces appeared to be generally lower throughout the hop cycle (Fig. 2E) and that there was a significant reduction in peak and average MG forces when exoskeletons were used (Fig. 3A, Table 1). Also, the use of spring-loaded exoskeletons resulted in a significantly shorter average MG fibre length output by the model (Fig. 2I, Fig. 3A, Table 1) and a shift in MG operating length down the ascending limb of its force–length relationship (Fig. 4A). Furthermore, the simulated average MG fibre velocity significantly increased when exoskeletons were used (Fig. 3A, Table 1). F_{ind} is the index of force-producing capability of a muscle and represents the ratio of the force being produced relative to the maximum force the muscle could produce given its active state (Eqn 1 – Materials and methods). Related to the above mechanical changes, F_{ind} for MG was significantly reduced when exoskeletons were worn (Fig. 3A, Table 1). The rate of positive mechanical work done by MG fibres was unchanged with exoskeletons, but the rate of negative work increased (Table 1). Time series group average data for MG activation (Fig. 2A) show that for the majority of ground contact (20–70% hop cycle), MG activation followed a similar trend and was of similar magnitude with and without exoskeletons. As a result, there was no difference in the MG peak or average activations between these conditions (Fig. 3A, Table 1).

Lateral gastrocnemius

LG activation, fibre force, fibre length and fibre velocity output from the simulations are plotted throughout the hop cycle in Fig. 2B,F,J,N. There were significant reductions in LG peak and average forces with exoskeletons (Fig. 3B, Table 1). No differences in average fibre length or velocity were observed with exoskeleton use for LG, although the F_{ind} of LG was reduced with exoskeletons (Fig. 3B, Table 1). Positive mechanical fibre work was unchanged with exoskeletons for LG (Fig. 3B, Table 1). Average and peak LG activations were unchanged for hopping with exoskeletons versus those without (Fig. 3B, Table 1).

Soleus

Similar to other plantar-flexors, the simulation results showed that SO demonstrated a significant reduction of average and peak forces when exoskeletons were used. Notably, the simulations revealed that there was a threefold increase in the average fibre shortening velocity for SO with exoskeletons and that SO operated at a significantly shorter average length under that condition (Fig. 3C, Table 1). This caused a rightward shift along the force–velocity relationship of SO (Fig. 5C) and a shift down the ascending limb of the force–length relationship when exoskeletons were used (Fig. 4C). The net result of these mechanical changes was a significantly lower F_{ind} value for SO for hopping in exoskeletons (Fig. 3C, Table 1). However, there was a significant decrease in the negative rate of work for SO fibres and MTU with exoskeletons, and this caused greater positive net work per hop (Table 1). SO average activation was significantly less with exoskeletons (−21%) although peak activation was unchanged (Fig. 3C, Table 1).

The Journal of Experimental Biology (2014) doi:10.1242/jeb.107656

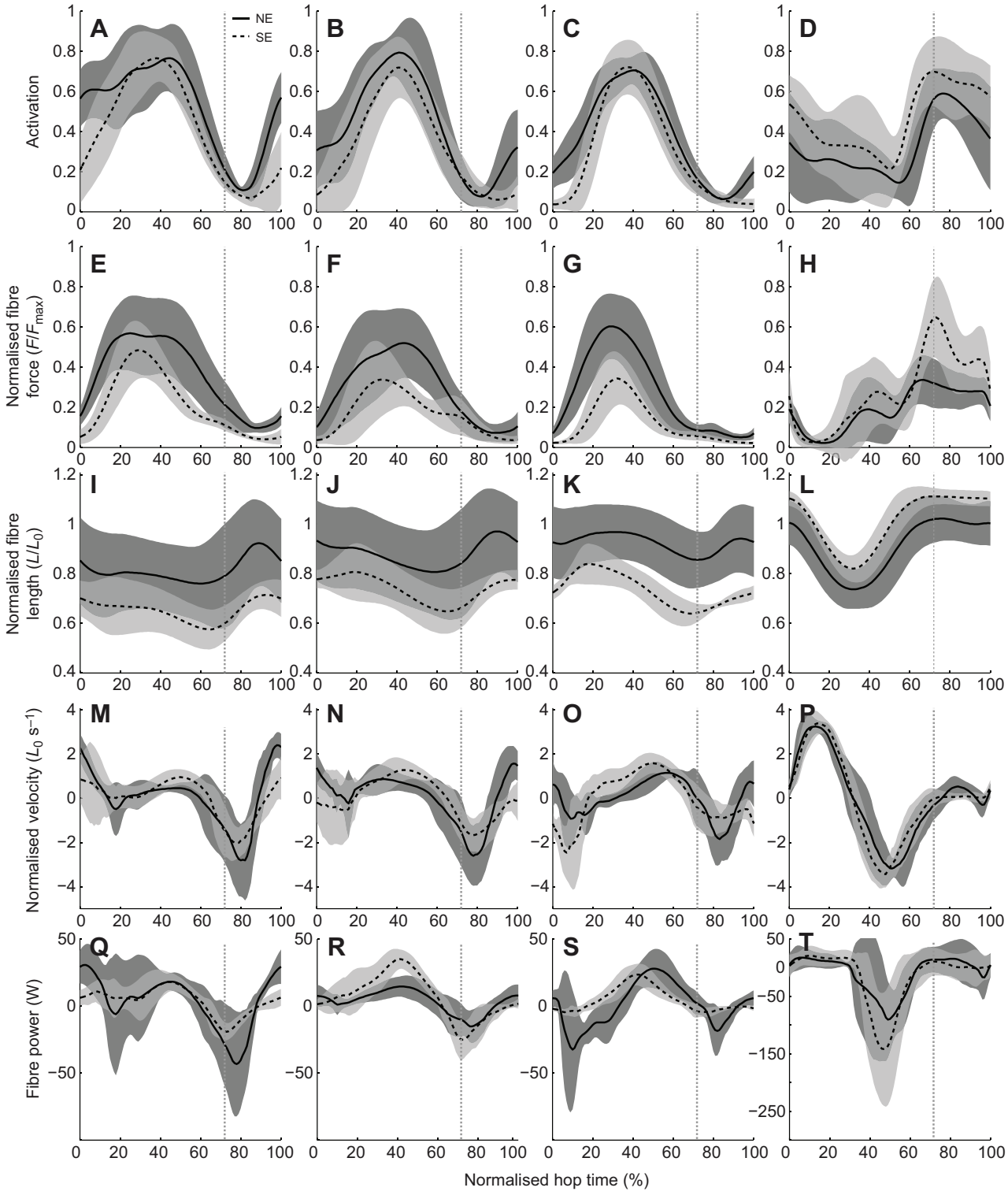

Fig. 2. Group mean (±s.d.) plots of modelled muscle activation, normalised fibre force, normalised fibre length, normalised fibre velocity and fibre power. (A–D) Modelled muscle activation, (E–H) normalised fibre force, (I–L) normalised fibre length, (M–P) normalised fibre velocity and (Q–T) fibre power for the (A,E,I,M,Q) medial gastrocnemius, (B,F,J,N,R) lateral gastrocnemius, (C,G,K,O,S) soleus and (D,H,L,P,T) tibialis anterior. Positive values for velocities correspond to shortening of muscle fibres. Solid lines represent the condition without exoskeletons (NE) and dashed lines the condition with spring-loaded exoskeleton (SE). Data are normalised to hop cycle time (0–100%), 0% representing landing and the dotted vertical lines indicating take-off. F, fibre force; F_{max}, muscle maximum isometric force; L, fibre length; L_0, optimum fibre length.

Tibialis anterior

Time series plots of simulated TA activation (Fig. 2D) and force (Fig. 2H) showed similar trends and magnitudes under both conditions during ground contact. This was evidenced further by the lack of difference in average or peak activations and forces for TA between hopping with exoskeletons and without (Fig. 3D, Table 1).

The Journal of Experimental Biology (2014) doi:10.1242/jeb.107656

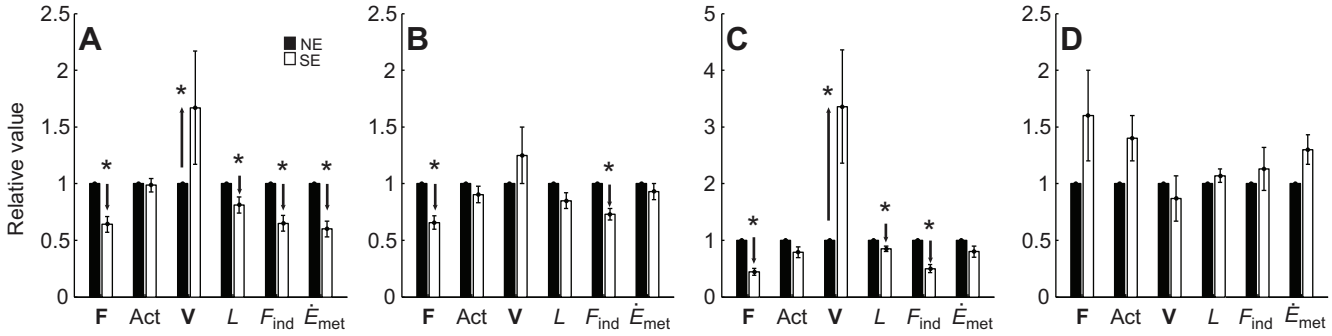

Fig. 3. Group mean (±s.d.) average fibre force (F), average activation (Act), average fibre velocity (V), average length (*L*), index of force producing ability (F_{ind}) and rate of metabolic energy consumption ($\dot{E}_{met}$) for muscles. (A) MG, (B) LG, (C) SO and (D) TA. Values are normalised to the value obtained under the condition without exoskeletons. Without exoskeletons (NE) is represented by black bars and with spring-loaded exoskeletons (SE) by white bars. Arrows with an asterisk indicate a significant change in that variable between NE and SE (P<0.05).

In fact, there were no significant differences in mechanical variables between conditions for TA (Fig. 3D, Table 1).

DISCUSSION

In this study we sought to mechanistically link changes in the mechanics of ankle muscles to changes in muscle energy consumption when humans hop with and without elastic ankle exoskeletons that assist plantar-flexion. Our first hypothesis was that plantar-flexor muscle forces would be reduced by the use of spring-loaded ankle exoskeletons. There was strong support for this hypothesis as peak and average forces were significantly less for all plantar-flexors (MG, LG and TA) when hopping was assisted with exoskeletons. Our second hypothesis was that the contractile work of the plantar-flexor muscles would not change with exoskeletons. This hypothesis was also supported, as there was no change in the positive fibre work for any of the plantar-flexors when hopping in exoskeletons due to a paradoxical trade-off between force production and fibre shortening. Finally, we hypothesised that ankle exoskeletons would reduce the rate of metabolic energy consumption by plantar-flexors through reduced forces and activations. This hypothesis was not supported because the combined rate of energy consumption and all individual muscle activations were not reduced to a statistically significant extent with exoskeletons.

Linking muscle mechanics and energetics

F_{ind} was our measure of how favourable the state of a muscle was for producing force given its fibre length and velocity. F_{ind} can be any value between 0 and 1, and the closer it is to 1, the less activation is required to produce a given force and the greater the maximum force that can be produced is. With exoskeletons, F_{ind} was significantly less than without for all the plantar-flexor muscles for the period of ±25% hop cycle time either side of the time of maximum force. This indicated that even though the forces required

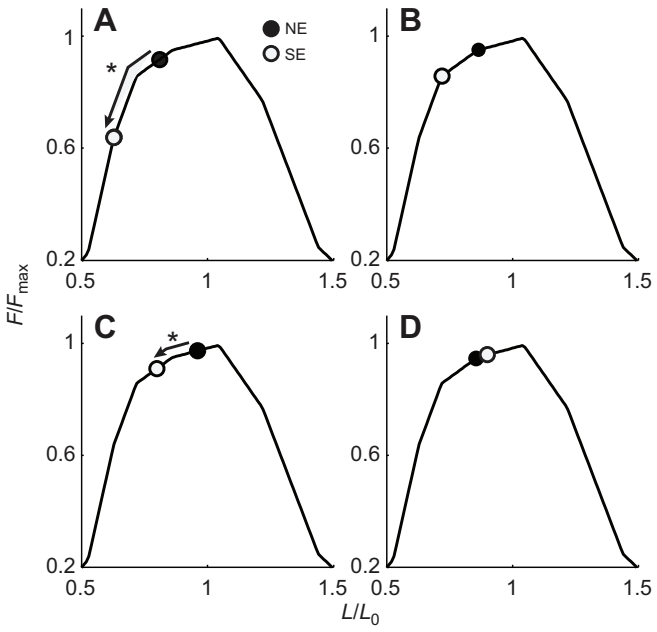

Fig. 4. The generic muscle model force–length relationship with the average operating lengths for each muscle shown without exoskeletons (NE) and with spring-loaded exoskeletons (SE) with filled and empty circles, respectively. (A) MG, (B) LG, (C) SO and (D) TA. (A,C) Arrows with an asterisk highlight a significant (P<0.05) left-shift down the ascending limb of the force–length relationship between NE and SE for MG and SO.

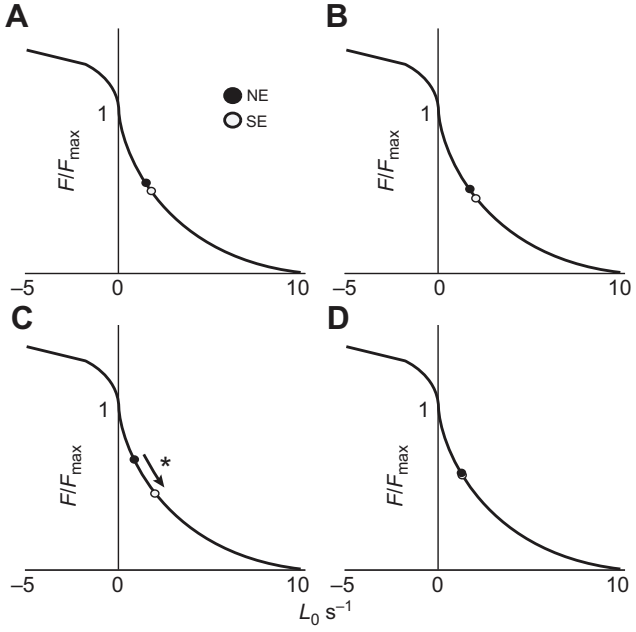

Fig. 5. The generic muscle model force–velocity relationship with the peak velocities for each muscle without exoskeletons (NE) and with spring-loaded exoskeletons (SE) plotted with filled and empty circles, respectively. (A) MG, (B) LG, (C) SO and (D) TA. (C) The arrow with an asterisk highlights a significant (P<0.05) right-shift along the force–velocity relationship between NE to SE for SO.

The Journal of Experimental Biology (2014) doi:10.1242/jeb.107656

of the plantar-flexors were reduced, their contractile elements were not in as favourable a state for producing force. This finding was further confirmed by inspection of plantar-flexor muscle velocities and lengths (Figs 3, 4, 5 and Table 1). In Fig. 2M–O, it can be seen that during periods of greatest force production, plantar-flexors reached higher shortening velocities with exoskeletons than without. This resulted in significantly higher average shortening velocities for MG and SO and a significantly higher peak shortening velocity for SO (Fig. 3A–C, Fig. 5C, Table 1). Faster shortening velocities reduce the force-generating capacity of muscle (Fenn and Marsh, 1935). Thus, the increased average velocities for MG and SO with exoskeletons contributes to the lower F_{ind} values observed for those muscles.

The length–tension relationship of skeletal muscle (Gordon et al., 1966) describes that at lengths above and below an optimum fibre length (L_0), the force producing capability of the muscle is impaired. As can be seen in Fig. 2, all the plantar-flexors consistently operated at fibre lengths less than L_0, and average fibre lengths were shorter for MG and SO with exoskeletons (Fig. 3A–C, Table 1). This shifted MG and SO fibre operating lengths down the ascending limb of the force–length relationship (Fig. 4A,C) where contractile elements have lower force-producing capacities. This shift also contributed to the lower F_{ind} values observed for MG and SO when hopping in exoskeletons. Although LG did not exhibit any significant changes in peak or average fibre lengths and velocities, it did demonstrate a reduced F_{ind} value when exoskeletons were used, which is likely to be due to a cumulative effect of small changes in LG length and velocity.

Despite average forces for MG, LG and SO muscles being 42%, 37% and 56% lower with exoskeletons (Fig. 3, Table 1), the expected concomitant reductions in muscle activation were offset by poor contractile conditions that required higher activation per unit force (i.e. reduced F_{ind}). In fact, of the plantar-flexors, only SO had a significantly lower average activation (Fig. 3, Table 1) and this was only reduced by 21% despite the SO average force being 56% less. Furthermore, positive muscle fibre work was not significantly altered for any of the plantar-flexors by exoskeletons (Table 1). The amount of fibre work is dependent upon the amount of shortening of a fibre and the force produced during that shortening. Because fibre force was reduced with exoskeletons but fibre shortening velocity (and therefore shortening) increased with exoskeletons, positive fibre work was unchanged. Thus, a trade-off between force and shortening velocity seems to occur for plantar-flexor muscles when hopping with and without assistance from a parallel spring. These findings agree well with our previous data that indicated SO force was reduced using exoskeletons but not SO fibre positive mechanical work (Farris et al., 2013). As can be seen from Table 1, the negative rate of work was significantly less when hopping in exoskeletons for MG and SO, but not LG, which exhibited more positive net fibre work per hop. An inspection of fibre length and force data in Fig. 2 reveals that this is likely to be due to reductions in force and activation of MG and SO when fibres are lengthening.

The changes we observed in muscle fascicle mechanics can be used to understand the factors that drive changes in the underlying metabolic energy consumption of individual ankle muscles during spring-assisted hopping. The model of muscle energetics produces rates of energy consumption based on inputs of mechanical fibre work, fibre forces, muscle activations and fibre velocities. Increases in any of these variables will generally increase rates of energy consumption (although not proportionally). Therefore, we can see that the computed reductions in the average and peak plantar-flexor forces with exoskeletons would serve to reduce the rates of energy consumption by these muscles. Fibre positive mechanical work was unchanged between conditions and thus had little influence on the relative rates of energy consumption with and without exoskeletons. However, the net rate of fibre work was more positive for LG and SO with exoskeletons; this will have served to increase the metabolic rate for these muscles and might be the reason why the metabolic rate was not significantly reduced for these muscles. This is in contrast to MG, in which the metabolic rate decreased and the net fibre work remained unchanged. This effect would have been somewhat mitigated by a concomitant reduction in the rate of negative work for the fibres of SO with exoskeletons. The average activation was only reduced by exoskeletons for SO. The final factor that determined energy consumption was fibre velocity and this significantly increased with exoskeletons for MG and SO, and did not change for LG (Fig. 3, Table 1). Thus, combined plantar-flexor fibre velocities would have served to increase the rates of energy consumption. In the case of SO, the velocity increased threefold with exoskeletons and thus may have acted to increase energy consumption sufficiently to override any reductions resulting from reduced SO activation. For LG, no changes were observed in activation or velocity and, as these terms dominate energy consumption in the energetics model (Eqns 4, 5), it is unsurprising that LG energy consumption was unchanged with exoskeletons. MG did have a lower rate of energy consumption with exoskeletons and this was primarily due to the effect of reduced force levels outweighing the effect of an increase in fibre velocity, which was somewhat less than the increase observed for SO (Fig. 3). However, SO is by far the largest of the plantar-flexors and therefore has the potential to dominate energy consumption by this muscle group. Therefore, the lack of change in SO energy consumption with exoskeletons washed out the reduction from MG when all muscles were combined. Of course, TA also contributed to the total energy consumption but showed no change in any mechanical or energetic variables (Fig. 3D, Table 1) and as such, contributed consistently across conditions.

Comparison to experimental hopping energetics

The model prediction of no significant reduction in the total rate of energy consumption seems at odds with our previous experimental measures of whole-body net metabolic power that did show a reduction when hopping in ankle exoskeletons (Farris and Sawicki, 2012a; Farris et al., 2013). A close inspection of the energetic model outputs shows that the total rate of energy consumption of all ankle muscles was 0.68 and 0.57 $J\,kg^{-1}\,hop^{-1}$ without and with exoskeletons, respectively. This gives a difference of 0.11 $J\,kg^{-1}\,hop^{-1}$ for the musculature of one ankle. In the previous experimental study, the whole-body net metabolic power was reduced by 0.9 $W\,kg^{-1}$ with exoskeletons compared with that without exoskeletons. Half of this reduction was attributed to reductions in knee power output (Farris et al., 2013), leaving 0.45 $W\,kg^{-1}$ attributable to changes in ankle muscle mechanics in both legs. Halving this value again gives us a net reduction of 0.225 $W\,kg^{-1}$ for the musculature of one ankle. Dividing this value by 2.5 (hopping frequency) returns a value of 0.09 $J\,kg^{-1}\,hop^{-1}$ that compares well with the prediction of the metabolic model. First, we note that in both analyses this is quite a small difference and only accounts for about half of the experimentally observed reduction in whole-body net metabolic power (Farris et al., 2013). Our previous inverse dynamic analysis suggests that the remaining metabolic reductions were likely to be a result of reduced mechanical power output at the knee joint when exoskeletons were worn (Farris and Sawicki, 2012a; Farris et al., 2013). This presents an interesting

scenario where an exoskeleton that directly assists at one joint may affect mechanical changes at other joints that impact upon the overall mechanical and metabolic demands of locomotion. Secondly, we note that the similarity of experimental and modelled energetic values gives us high confidence in our energetic model predictions, even though the simulation results showed no significant difference between conditions. It may be that our statistical power was insufficient to detect a statistically significant reduction when the reduction is of a relatively small magnitude. We therefore suggest that ankle exoskeletons may not totally fail to reduce the metabolic energy consumption of ankle muscles but rather that the paradoxical trends in muscle mechanics limit the reduction to being quite small and, in our case, not statistically significant.

Model evaluation

To evaluate our simulations of muscle–tendon dynamics, we employed the same approach as Arnold et al. (Arnold et al., 2013) and compared ankle joint kinetics to those computed by inverse dynamic solutions using the same experimental data. As shown in Fig. 1 and Table 2, ankle moments and powers showed good temporal agreement between inverse solutions and simulations, and generally a non-significant shortfall in magnitudes. One might expect the simulations to under-predict muscle forces and thus moments and powers. This is owing to the fact that the muscle maximum isometric force (F_{max}) was not scaled to individual participants. The model parameter values for muscle properties came from cadavers with a mean age of 83±9 years, including a mixture of male and female specimens (Ward et al., 2009). The experimental group used for the current study comprised young (mean age: 28±7 years) physically active males who were likely to have larger and/or stronger muscles than the cadaver specimens. Thus, it was not surprising that the magnitudes of ankle moments and powers were quantitatively less in the muscle–tendon dynamic simulations. However, the temporal agreement was good, and the magnitudes were generally within one standard deviation of each other, giving us high confidence in the simulations of muscle–tendon dynamics.

This confidence was increased further because similar trends in SO muscle mechanics between conditions were predicted by the model as were observed in recent experimental data collected using ultrasound imaging to measure SO fascicle length changes when hopping in ankle exoskeletons (Farris et al., 2013). The fascicle length changes represent lumped length changes of the muscle contractile elements, as does fibre length in the musculoskeletal model. Therefore the terms fascicle and fibre will be considered interchangeable in this discussion, even though they may have distinct anatomical definitions. Both simulated and experimental data showed that fibre length changes increased significantly with exoskeletons (Fig. 1E,F). This similarity was most important for providing confidence that our model was appropriate for our research question, which was related to the effects of exoskeletons. However, there were some discrepancies in the length change patterns of simulated and experimental fascicle lengths. The gross length change pattern for simulations and experimental data was lengthening followed by shortening over ground contact and then a return to the starting length during the aerial phase. However, the period of fibre shortening began somewhat earlier in the simulations (Fig. 1E–H), and length changes were generally larger in the simulations. Exact quantitative agreement between the simulated and experimental fibre lengths might be unrealistic to obtain given that the exact properties of participant's muscles were unknown and the model is a simplification of reality. Muscle dynamics were relatively insensitive to changes in muscle parameters (supplementary material Figs S1–S3) and, as noted earlier, the simulated effects of exoskeletons were comparable to experimental findings in terms of muscle dynamics and metabolic data. A noteworthy discrepancy between the experimental and simulation datasets was that the simulations showed that exoskeletons reduced the SO average fibre length, whereas experimental data showed no change in the average fascicle length [table 1 in Farris et al. (Farris et al., 2013)]. The whole SO MTU length was reduced with exoskeletons because the ankle was more plantar-flexed throughout the hops under this condition. The experimental data showed this length change to occur entirely through shortening of series elastic structures (i.e. the Achilles tendon), allowing the SO fascicles to be at the same average length with and without exoskeletons. However, the simulations showed that both the SO tendon and fibres had shorter average lengths when exoskeletons were worn. A plausible explanation for this discrepancy is that the SO tendon compliance set in the musculoskeletal model was too great. A less compliant tendon would have been stretched less by the forces applied by SO; thus, the muscle fibre length would have shortened less or not at all. An overly compliant tendon might also explain why SO fibre length changes were slightly greater in the simulation results than in the experimental data. Tendon strain at F_{max} values for the plantar-flexors (T_{strain} in Table 3) were determined such that, when acting in parallel, the combined stiffness of the MG, LG and SO tendons would match an experimentally determined value for Achilles tendon stiffness of 180 N mm^{-1} (Lichtwark and Wilson, 2005b). This is a simplification of the real anatomy where the three muscles insert through a common tendon of this stiffness. Achilles tendon compliance may also vary greatly between individuals (Lichtwark and Wilson, 2005b) and be inversely proportional to muscle strength (Muraoka et al., 2005). Given that the participants in the experimental data collection were young physically active males, it is possible that the average tendon compliance of this group would be less than that that of previously published data from participant groups with potentially lesser muscle strength. However, repeating the simulations with a 10% stiffer tendon in each muscle, for one of the scaled models, produced only marginally shorter fibre lengths during hopping and minimal changes in other outcome measures (supplementary material Fig. S1). Therefore, we believe our findings to be relatively insensitive to tendon compliance and that any effect would be systematic across experimental conditions.

Generally the musculoskeletal model performed well, and we believe it capable of accurately predicting the effects of ankle

Table 2. Comparison of ankle kinetics from the muscle-tendon dynamics simulations and inverse dynamics solutions

	No exoskeleton		Exoskeleton	
	Simulations	Inverse dynamics	Simulations	Inverse dynamics
Peak ankle moment (Nm kg^{-1})	−1.48±0.41	−1.74±0.40	−1.49±0.30	−1.99±0.50
Time of peak moment (% hop cycle)	32±7	34±5	32±5	34±4
Peak ankle power (W kg^{-1})	4.2±1.8	4.4±1.4	4.8±1.5	6.1±2.3
Time of peak power (% hop cycle)	49±7	47±7	45±7	44±4

Table 3. Muscle properties of the generic model

	M. gastrocnemius	L. gastrocnemius	Soleus	Tibialis anterior	Source
F_{max} (N)	1308	606	3586	1375*	(Arnold et al., 2010) (Raasch et al., 1997)*
V_{max} (L_0 s^{-1})	10	10	10	10	(Zajac and Gordon, 1989)
L_0 (m)	0.051	0.059	0.044	0.049	(Arnold et al., 2010)
T_s (m)	0.40	0.38	0.28	0.31	(Arnold et al., 2010)
T_{strain} (%)	10	10	11	9	Calculated
τ_{act}	0.011	0.009	0.031	0.015	(Winters and Stark, 1988)
τ_{deact}	0.045	0.038	0.111	0.055	(Winters and Stark, 1988)

*The F_{max} of tibialis anterior was adjusted to include the force-producing capability of all dorsi-flexors, as per Raasch et al. (Raasch et al., 1997). T_s, tendon slack length; T_{strain}, tendon strain at F_{max}; τ_{act} and τ_{deact}, time constant for activation and deactivation, respectively; V_{max}, maximum shortening rate of the contractile element of the muscle.

exoskeletons on ankle muscle mechanics during hopping. This is despite some limitations of the muscle model, which include not accounting for variable gearing of pennate muscles (Azizi et al., 2008), force depression after shortening and stretch-induced force enhancement (Julian and Morgan, 1979), changes in the force–velocity and force–length relations that occur with submaximal activation (Rack and Westbury, 1969), three-dimensional structure or non-homogenous structure (Huijing, 1998). Each of these factors could affect muscle force predictions. Azizi et al. (Azizi et al., 2008) have shown that pennate muscle, such as the triceps surae, might rotate their fibres more during low force–high velocity contractions and keep them more aligned with the muscle line of action during high force–low velocity contractions (variable gearing). The exoskeletons reduced muscle forces, which would place the muscles more towards the low force–high velocity end of this spectrum; thus, a model incorporating variable gearing would be likely to predict greater fascicle rotation under the exoskeleton condition, which would only serve to further reduce force along the line of action of the MTU by making the fibres more oblique to it. Residual force enhancement would suggest that after a stretch, muscle fibres are able to produce more force at a given length. There was generally more stretch of muscle fibres of the plantar flexors with exoskeletons, and thus the difference in forces between the two conditions might have been affected had force enhancement been included in the muscle model. The skeletal muscle force–length relation shifts to the right (longer optimal length) at submaximal activations, and this is not accounted for in the muscle model. Because of the dynamic interaction between length, force and activation, it is difficult to predict what the effects of accounting for this might be. Generally, lower activations and shorter lengths of fibres were observed with exoskeletons, which would suggest that the difference in forces between the conditions might have been greater than those observed owing to a more rightward shift of optimal length and shorter predicted lengths of fibres with exoskeletons. The energetics model has been carefully validated against experimental data previously (Lichtwark and Wilson, 2005a). This and the good agreement with experimental metabolic data from this study (discussed in detail above) also gave us confidence in our energetic predictions.

Conclusions

Using a musculoskeletal model we have shown that spring-loaded ankle exoskeletons can negatively influence plantar-flexor muscle mechanics during bilateral hopping. The negative effects were: (1) increased muscle fibre shortening velocity and (2) a shift in the average operating length down the ascending limb of the force–length relationship. As a result, the mechanical work done by muscle fibres was not reduced by exoskeletons, and these devices caused only limited reductions in plantar-flexor muscle activations. Consequently, our energetics model predicted that only MG consumed less energy with exoskeletons and that ankle muscle energy consumption was not significantly reduced by spring-loaded ankle exoskeletons. This indicates that experimentally observed reductions in whole-body net metabolic cost are heavily influenced by the effects of ankle exoskeletons at other joints, as well as those on ankle musculature.

MATERIALS AND METHODS

Experimental data

The musculoskeletal modelling required experimental data as input to the simulations of muscle–tendon dynamics. The data included kinematic, ground reaction force (GRF) and surface EMG recordings. This data was taken from the results of a previously published study (Farris and Sawicki, 2012a), which describes the data collection procedures and the ankle exoskeleton design in detail. Briefly, seven male participants (mean ± s.d.; age, 28±7 years; height, 1.8±0.06 m; mass, 80±10 kg) hopped bilaterally under two conditions: (1) without exoskeletons and (2) with spring-loaded ankle exoskeletons to assist plantar-flexion. The exoskeletons comprised a carbon fibre foot section embedded in a running shoe and a carbon fibre cuff around the shank, which were connected by aluminium bars via a freely rotating joint aligned with the malleoli. When spring-loaded, a spring was attached to a bracket on the posterior aspect of the cuff and a bolt on the heel of the foot segment. The rotational stiffness provided about the ankle joint by the spring was calculated as 91 N m rad^{-1}. The spring was at its resting length when the ankle was at an angle of 129 deg (foot segment relative to the shank segment; at 90 deg, the foot was perpendicular to the shank).

Participants hopped at 2.5 Hz in time with a metronome. Reflective markers were placed over the right leg and pelvis [see Farris and Sawicki (Farris and Sawiki, 2012a) for details of placements] and their trajectories captured and labelled using an eight-camera Vicon motion analysis system and Vicon Nexus software (Vicon, UK). The same system synchronously recorded GRF data from the left and right legs, which were measured using each half of a split-belt instrumented treadmill (Bertec, OH, USA). Also logged synchronously were surface EMG signals from the MG, LG, SO and TA muscles. Raw EMG signals were processed in MATLAB (The MathWorks, MA, USA) with a band-pass filter (20–300 Hz) and a moving average root mean square calculation made over successive windows of 20 ms. Processed signals were then normalised to the average peak (in each hop, from a series of 10 hops) of the processed signal from the condition where the signal of that muscle had the greatest peaks (i.e. with exoskeletons for MG, LG and SO; without exoskeletons for TA).

Musculoskeletal model

The generic musculoskeletal model (Fig. 6A) was adapted from the model of the pelvis and lower limb published previously by Arnold et al. (Arnold et al., 2010) that has been used to produce dynamic simulations of human walking and running (Arnold and Delp, 2011; Arnold et al., 2013) and to analyse lower limb muscle function during locomotion (Arnold and Delp, 2011; Arnold et al., 2013). Here, we were only interested in the mechanics of a subset of the 35 muscles included in the original model: MG, LG, SO

The Journal of Experimental Biology (2014) doi:10.1242/jeb.107656

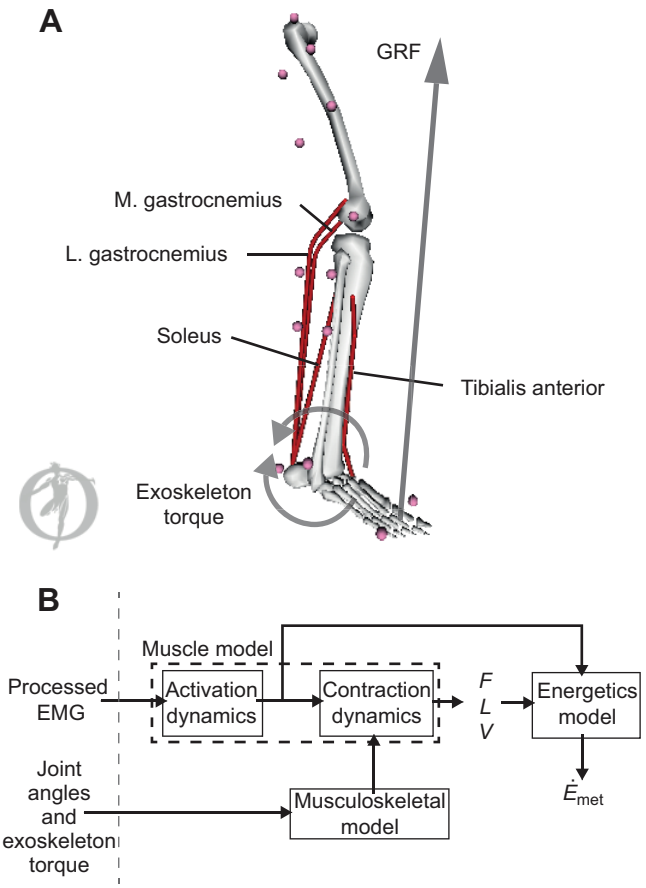

Fig. 6. Overview of the modelling process. (A) The musculoskeletal model adapted from Arnold et al. (Arnold et al., 2010). The exoskeleton torque from the experimental data was applied as equal and opposite torques acting on the shank and foot. The ground reaction force (GRF, grey arrow) and markers used to determine the joint angles for the ankle and knee (pink spheres) are also shown. (B) Schematic giving an overview of the integration of experimental EMG and kinematic (joint angle) data into the modelling process. Processed EMG signals were considered as excitations and fed into a first order model of activation dynamics to produce activations. Experimentally determined joint angles were input to the musculoskeletal model to compute MTU lengths. Activations and MTU lengths were combined in an equilibrium model of contraction dynamics to calculate muscle fibre force (*F*), fibre length (*L*) and fibre velocity (*V*). *F*, *L*, *V* and activations served as inputs to the energetics model to compute the rate of metabolic energy consumption ($\dot{E}_{met}$). GRF, ground reaction force.

and TA. Because we prescribed joint angles during the simulations of muscle–tendon dynamics (see Musculoskeletal simulations), it was unnecessary to model the other lower limb muscles. Therefore, we removed all muscles except those listed above from the model. Consequently, there were no muscles in the model attached to the pelvis and so the pelvis segment was removed. The rigid bodies in the model included thigh (femur and patellar), shank (tibia and fibula) and foot (talus, calcaneus metatarsals and phalanges) segments. The geometry of the segments was from the digitisation of the bones of an adult male (Delp et al., 1990). Articulation between segments was possible at the knee and ankle joints. The ankle was a revolute joint between the tibia and talus with one degree of freedom (plantar-flexion and dorsi-flexion) (Inman, 1976; Arnold and Delp, 2011). The knee joint also had one rotational degree of freedom (flexion and extension) with translations and rotations between the femur, patellar and tibia being described by the equations from Walker et al. (Walker et al., 1988) and Delp (Delp, 1990). A joint between the thigh and the laboratory coordinate system was created with six degrees of freedom to allow the leg to translate and rotate relative to the laboratory.

The path of each muscle was modelled by line segments between the origin and insertion that included wrapping surfaces and points to account for parts of those paths where the muscle wraps over bones or other muscles, or is constrained by retinacula (Arnold et al., 2010). Each muscle was modelled as a Hill-type muscle with a single fibre in series with a series elastic element (subsequently referred to as tendon). Muscle parameters are described in Table 3. Architectural muscle parameters were optimal fibre length (L_0), pennation at optimal fibre length (α_0) and tendon slack length (T_s). L_0 and α_0 were taken from a study of 21 cadavers (Ward et al., 2009) and T_s values were as defined previously by Arnold et al. (Arnold et al., 2013) who used the joint positions and fibre lengths from Ward et al. (Ward et al., 2009) to set T_s. The F_{max} of each of the plantar-flexors was taken from Arnold et al. (Arnold et al., 2010) who calculated F_{max} from the physiological cross-sectional areas reported by Ward et al. (Ward et al., 2009) and a specific tension for muscle of 61 N cm^{-2}. The F_{max} of TA was increased from the value in Arnold et al. (Arnold et al., 2010) to that reported by Raasch et al. (Raasch et al., 1997) so as to include the force-producing capabilities of other dorsi-flexors (Table 3). This was done to produce realistic ankle joint moments and powers during periods of co-contraction of plantar-flexors and dorsi-flexors. Architectural muscle parameters were used to scale normalised curves relating active force, passive force and tendon force to muscle kinematics (e.g. Zajac and Gordon, 1989; Millard et al., 2013). Scaled curves provided multipliers to, in combination with activation level, determine muscle fibre and tendon force from normalised fibre length, shortening velocity and tendon strain (Zajac and Gordon, 1989). The normalised curves for active force–length and force–velocity were modelled with natural cubic splines (Zajac and Gordon, 1989; Arnold et al., 2013). The maximum shortening velocity was set to 10 L_0 s^{-1} for all muscles. Passive force–length and tendon force–strain were represented by exponential functions (Thelen, 2003; Arnold et al., 2013). Detailed equations for this process are described in Arnold et al. (Arnold et al., 2013). The tendon force–strain relationship is dictated by the tendon strain at F_{max}. Often, this strain value has been set to 0.03 for all muscles. However, the muscles surrounding the human ankle joint typically have long compliant tendons that experience larger strains. Arnold et al. (Arnold et al., 2013) found previously that strain at F_{max} for ankle muscles needed to be increased to 0.10 to yield reasonable ankle kinetics in their simulations of muscle–tendon dynamics. Here, we set the strain at F_{max} values for the plantar-flexors to values that, when combined (in parallel), would produce an Achilles tendon stiffness similar to that reported previously in experimental studies (Lichtwark and Wilson, 2005b; Farris et al., 2012). TA tendon strain at F_{max} was also set such that its stiffness was similar to experimental data (Maganaris, 2002). These values were all close to 0.10 (Table 3). The sensitivity of model outputs (muscle dynamics and metabolic energy consumption) to the input parameter values of T_{strain}, F_{max} and V_{max} was tested by repeating simulations having altered these parameters by ±10% of the values in Table 3. The results of these simulations are shown in the supplementary information (supplementary material Figs S1–S3, Table S1).

Musculoskeletal simulations

OpenSim software (v3.0) (Delp et al., 2007) was used to generate simulations of muscle dynamics during hopping at 2.5 Hz with and without spring-loaded ankle exoskeletons for the seven participants described above. For each participant, data from a series of 10 consecutive hops was analysed in each condition. First, the generic musculoskeletal model was scaled to match individual participant anthropometrics. This was done using distances between motion capture markers positioned on segment end points during quiet standing. Muscle L_0 and T_s were scaled with MTU lengths such that the ratio L_0/T_s remained the same as in the generic model. Next, previously collected motion capture data (Farris and Sawicki, 2012a) were used in conjunction with the scaled musculoskeletal models to determine model joint angles via an inverse kinematic solution to best fit the experimental data. This generated knee and ankle joint angles, as well as translations and rotations of the thigh in the laboratory. Next, the inverse kinematic solution was combined with GRF data in an inverse dynamics analysis to determine ankle plantar-dorsi flexion net moments and the power generated by those moments. These moments and powers were compared to the net moments

and powers generated by the muscles in the model during the simulations of muscle–tendon dynamics to evaluate the simulations. The inverse kinematics and dynamics data were computed with the current models and are therefore not identical to the previously published joint mechanics data in Farris and Sawicki (Farris and Sawicki, 2012a).

As can be seen from Fig. 6B, the experimental inputs to the simulations were: joint kinematics, exoskeleton torques and muscle electromyograms. The latter two of these were taken from Farris and Sawicki (Farris and Sawicki, 2012a). The inverse kinematic solutions described above were used to prescribe coordinates (translational and rotational) for the model joints in simulations of muscle–tendon dynamics, run with the scaled musculoskeletal models (Fig. 6B) and effectively determined muscle–tendon unit lengths. To simulate the contribution of the exoskeletons, experimentally determined moments produced by the exoskeleton about the ankle joint (Farris and Sawicki, 2012a) were applied as equal and opposite moments on the shank and foot segments of the model. An overview of how experimental data was integrated into the models is shown in Fig. 6B. Processed surface EMG signals (see Experimental data) were considered as muscle excitations and passed to an activation dynamics model to determine muscle activations. This model was a non-linear first order differential equation as used by Thelen (Thelen, 2003), which includes different time constants for activation (τ_{act}) and deactivation (τ_{deact}). We adjusted these time constants to match experimental muscle-specific data (Winters and Stark, 1988) (Table 3). Bounds were set on the activation signals such that they could not exceed 1 or fall below 0.01. Muscle activations and kinematic data served as inputs to the model of contraction dynamics described above. Outputs from the simulations included muscle fibre and tendon forces and muscle fibre and tendon kinematics. As a metric of the force-producing potential of each muscle, we calculated an index of force producing ability (F_{ind}). This index is described by Arnold et al. (Arnold et al., 2013) and is calculated as:

$$F_{ind} = \frac{\mathbf{F}_T}{\text{Act} \cdot F_{max}}, \quad (1)$$

where, F_{ind} is the index of force producing capability, F_T is the active force generated along the line of the tendon, Act is activation and F_{max} is the muscle's maximum isometric force. F_T depends on the normalised length and velocity of the muscle fibre and its pennation angle (Arnold et al., 2013).

Energetics model

Having determined muscle fibre forces and kinematics, and using the same values for individual muscle parameters as those in the musculoskeletal model, we employed a previously published and validated model of muscle energetics (Lichtwark and Wilson, 2005a) to predict individual muscle metabolic energy consumption. This model calculates the energy consumed by the contractile element of a muscle as the sum of mechanical work and heat production. Work is defined as being positive when the muscle fibre produces force while shortening (positive fibre velocities) and negative when the fibre produces force while lengthening (negative fibre velocities). To determine muscle fibre net mechanical work, fibre force was multiplied with fibre velocity to compute fibre power that was subsequently integrated with respect to time over a trial. Detailed descriptions of the equations used to calculate heat production are given in the supplementary information of Lichtwark and Wilson (Lichtwark and Wilson, 2007). Briefly, there were two main heat terms to compute – maintenance heat rate and shortening heat rate. Maintenance heat rate was determined as:

$$\frac{dH_m}{dt} = \gamma\left(\frac{V_{max}}{G^2}\right), \quad (2)$$

for $\mathbf{V}_{CE}>0$ and:

$$\frac{dH_m}{dt} = 0.3\left(\gamma\left(\frac{V_{max}}{G^2}\right)\right) + 0.7\left(\gamma\left(\frac{V_{max}}{G^2}\right) \cdot e^{-7V_{max}(P-1)}\right). \quad (3)$$

Shortening heat rate was determined as:

$$\frac{dH_s}{dt} = \left(\frac{\mathbf{V}_{CE}}{G}\right), \quad (4)$$

for $\mathbf{V}_{CE}>0$, and:

$$\frac{dH_s}{dt} = -0.5P \cdot \mathbf{V}_{CE}, \quad (5)$$

for $\mathbf{V}_{CE}<0$.

Total heat (H) was the sum of maintenance and shortening heat scaled by activation (Act) and the fraction of bound cross-bridges (X):

$$X = P(l) \cdot \text{Act}, \quad (6)$$

$$\frac{dH}{dt} = 0.3\text{Act}\left(\frac{dH_m}{dt}\right) + 0.7X\left(\frac{dH_m}{dt}\right) + X\left(\frac{dH_s}{dt}\right), \quad (7)$$

where $\mathbf{V}_{CE}$ is contractile component velocity relative to V_{max}, H_m is maintenance heat, γ is a constant (1.5) multiplier of stable heat rate to account for its labile component, V_{max} is the maximum shortening rate of the muscle's contractile element (10 L_0 s^{-1}), G is a constant (4.0) that determines the curvature of the muscle's force–velocity curve, P is the force produced relative to the maximum active force that can be produced at the current contractile element velocity (from the force–velocity curve), $P(l)$ is the maximum force that can be produced at a given contractile element length relative to F_{max}.

Total heat was integrated over a trial with respect to time and summed with net mechanical work to give the total energy consumed by each muscle. The energy consumed by all muscles was summed to give total energy consumption of the ankle muscles. All values for energy consumption were divided by body mass and the number of hops to give a rate of energy consumption in J kg^{-1} hop^{-1}.

Data reduction and statistics

Time series data for muscle mechanics were split up into individual hops based on vertical ground reaction force data and normalised to 101 evenly spaced points over each hop cycle. The averages of all hops for each subject were then computed and used to calculate group averages and standard deviations that were plotted against normalised hop time (e.g. Fig. 2). Peak muscle forces, activations, lengths and velocities were calculated in each hop and averaged across all hops within a subject and then across subjects. Average muscle forces, activations, lengths and velocities were computed for a period spanning ±25% of the hop cycle, either side of the occurrence of peak muscle force (for that muscle). F_{ind} was calculated from these values of average force and activation. Muscle mechanics data were normalised to either maximal activation (activation), F_{max} (forces) or L_0 (lengths and velocities) for that muscle. All data presented are group means and standard deviations unless otherwise stated. To test for differences in outcome variables between hopping with and without exoskeletons, Student's paired t-tests and an α level less than 0.05 were used as the criteria for statistical significance.

Acknowledgements

The authors would like to acknowledge Glen Lichtwark (The University of Queensland, Australia) for his assistance in implementing the model of muscle energetics.

Competing interests

The authors declare no competing financial interests.

Author contributions

D.J.F., G.S.S. and J.L.H. contributed to the conception of this project. D.J.F., G.S.S. S.L.D. and J.L.H. contributed to the design and interpretation of the musculoskeletal simulations, as well as drafting and revising the article. D.J.F. executed the musculoskeletal simulations and metabolic modelling.

Funding

This work was supported by the Visiting Scholars Program of The National Center for Simulation in Rehabilitation Research (NCSRR). The NCSRR is a National Center for Medical Rehabilitation Research supported by National Institutes of Health (NIH) research infrastructure grant [R24 HD065690]. This study was in part funded by US Israel Binational Science Foundation Start Up Grant [2011152] awarded to G.S.S. Deposited in PMC for release after 12 months.

Supplementary material

Supplementary material available online at
http://jeb.biologists.org/lookup/suppl/doi:10.1242/jeb.107656/-/DC1

References

Alexander, R. (1988). *Elastic Mechanisms in Animal Movement*. Cambridge: Cambridge University Press.

Arnold, E. M. and Delp, S. L. (2011). Fibre operating lengths of human lower limb muscles during walking. *Philos. Trans. R. Soc. B* **366**, 1530-1539.

Arnold, E. M., Ward, S. R., Lieber, R. L. and Delp, S. L. (2010). A model of the lower limb for analysis of human movement. *Ann. Biomed. Eng.* **38**, 269-279.

Arnold, E. M., Hamner, S. R., Seth, A., Millard, M. and Delp, S. L. (2013). How muscle fiber lengths and velocities affect muscle force generation as humans walk and run at different speeds. *J. Exp. Biol.* **216**, 2150-2160.

Azizi, E., Brainerd, E. L. and Roberts, T. J. (2008). Variable gearing in pennate muscles. *Proc. Natl. Acad. Sci. USA* **105**, 1745-1750.

Bobbert, M. F. (2014). Effect of unloading and loading on power in simulated countermovement and squat jumps. *Med. Sci. Sports Exerc.* **46**, 1176-1184.

Bregman, D. J. J., Harlaar, J., Meskers, C. G. M. and de Groot, V. (2012). Spring-like Ankle Foot Orthoses reduce the energy cost of walking by taking over ankle work. *Gait Posture* **35**, 148-153.

Cavagna, G. A. (1977). Storage and utilization of elastic energy in skeletal muscle. *Exerc. Sport Sci. Rev.* **5**, 89-130.

Delp, S. (1990). *Surgery Simulation: a Computer Graphics System to Analyze and Design Musculoskeletal Reconstructions of the Lower Limb.* PhD thesis, Stanford University, USA.

Delp, S. L., Loan, J. P., Hoy, M. G., Zajac, F. E., Topp, E. L. and Rosen, J. M. (1990). An interactive graphics-based model of the lower extremity to study orthopaedic surgical procedures. *IEEE Trans. Biomed. Eng.* **37**, 757-767.

Delp, S. L., Anderson, F. C., Arnold, A. S., Loan, P., Habib, A., John, C. T., Guendelman. E. and Thelen, D. G. (2007). Opensim: open-source software to create and analyze dynamic simulations of movement. *IEEE Trans. Biomed. Eng.* **54**, 1940-1950.

Farris, D. J. and Sawicki, G. S. (2012a). Linking the mechanics and energetics of hopping with elastic ankle exoskeletons. *J. Appl. Physiol.* **113**, 1862-1872.

Farris, D. J. and Sawicki, G. S. (2012b). Human medial gastrocnemius force-velocity behavior shifts with locomotion speed and gait. *Proc. Natl. Acad. Sci. USA* **109**, 977-982.

Farris, D. J., Trewartha, G. and McGuigan, M. P. (2012). The effects of a 30-min run on the mechanics of the human Achilles tendon. *Eur. J. Appl. Physiol.* **112**, 653-660.

Farris, D. J., Robertson, B. D. and Sawicki, G. S. (2013). Elastic ankle exoskeletons reduce soleus muscle force but not work in human hopping. *J. Appl. Physiol.* **115**, 579-585.

Fenn, W. O. and Marsh, B. S. (1935). Muscular force at different speeds of shortening. *J. Physiol.* **85**, 277-297.

Ferris, D. P., Bohra, Z. A., Lukos, J. R. and Kinnaird, C. R. (2006). Neuromechanical adaptation to hopping with an elastic ankle-foot orthosis. *J. Appl. Physiol.* **100**, 163-170.

Fukunaga, T., Kubo, K., Kawakami, Y., Fukashiro, S., Kanehisa, H. and Maganaris, C. N. (2001). In vivo behaviour of human muscle tendon during walking. *Proc. R. Soc. B* **268**, 229-233.

Gordon, A. M., Huxley, A. F. and Julian, F. J. (1966). The variation in isometric tension with sarcomere length in vertebrate muscle fibres. *J. Physiol.* **184**, 170-192.

Grabowski, A. M. and Herr, H. M. (2009). Leg exoskeleton reduces the metabolic cost of human hopping. *J. Appl. Physiol.* **107**, 670-678.

Huijing, P. A. (1998). Muscle, the motor of movement: properties in function, experiment and modelling. *J. Electromyogr. Kinesiol.* **8**, 61-77.

Inman, V. T. (1976). *The Joints of the Ankle*. Baltimore, MD: Williams and Wilkins.

Ishikawa, M., Komi, P. V., Grey, M. J., Lepola, V. and Bruggemann, G. P. (2005). Muscle-tendon interaction and elastic energy usage in human walking. *J. Appl. Physiol.* **99**, 603-608.

Julian, F. J. and Morgan, D. L. (1979). The effect on tension of non-uniform distribution of length changes applied to frog muscle fibres. *J. Physiol.* **293**, 379-392.

Lichtwark, G. A. and Wilson, A. M. (2005a). A modified Hill muscle model that predicts muscle power output and efficiency during sinusoidal length changes. *J. Exp. Biol.* **208**, 2831-2843.

Lichtwark, G. A. and Wilson, A. M. (2005b). In vivo mechanical properties of the human Achilles tendon during one-legged hopping. *J. Exp. Biol.* **208**, 4715-4725.

Lichtwark, G. A. and Wilson, A. M. (2006). Interactions between the human gastrocnemius muscle and the Achilles tendon during incline, level and decline locomotion. *J. Exp. Biol.* **209**, 4379-4388.

Lichtwark, G. A. and Wilson, A. M. (2007). Is Achilles tendon compliance optimised for maximum muscle efficiency during locomotion? *J. Biomech.* **40**, 1768-1775.

Lichtwark, G. A., Bougoulias, K. and Wilson, A. M. (2007). Muscle fascicle and series elastic element length changes along the length of the human gastrocnemius during walking and running. *J. Biomech.* **40**, 157-164.

Maganaris, C. N. (2002). Tensile properties of in vivo human tendinous tissue. *J. Biomech.* **35**, 1019-1027.

Millard, M., Uchida, T., Seth, A. and Delp, S. L. (2013). Flexing computational muscle: modeling and simulation of musculotendon dynamics. *J. Biomech. Eng.* **135**, 021005.

Muraoka, T., Muramatsu, T., Fukunaga, T. and Kanehisa, H. (2005). Elastic properties of human Achilles tendon are correlated to muscle strength. *J. Appl. Physiol.* **99**, 665-669.

Raasch, C. C., Zajac, F. E., Ma, B. and Levine, W. S. (1997). Muscle coordination of maximum-speed pedaling. *J. Biomech.* **30**, 595-602.

Rack, P. M. H. and Westbury, D. R. (1969). The effects of length and stimulus rate on tension in the isometric cat soleus muscle. *J. Physiol.* **204**, 443-460.

Thelen, D. G. (2003). Adjustment of muscle mechanics model parameters to simulate dynamic contractions in older adults. *J. Biomech. Eng.* **125**, 70-77.

Umberger, B. R. and Rubenson, J. (2011). Understanding muscle energetics in locomotion: new modeling and experimental approaches. *Exerc. Sport Sci. Rev.* **39**, 59-67.

Walker, P. S., Rovick, J. S. and Robertson, D. D. (1988). The effects of knee brace hinge design and placement on joint mechanics. *J. Biomech.* **21**, 965-974.

Ward, S. R., Eng, C. M., Smallwood, L. H. and Lieber, R. L. (2009). Are current measurements of lower extremity muscle architecture accurate? *Clin. Orthop. Relat. Res.* **467**, 1074-1082.

Wiggin, M. B., Collins, S. H. and Sawicki, G. S. (2011). An exoskeleton using controlled energy storage and release to aid ankle propulsion. In *IEEE International Conference on Rehabilitation Robotics*, pp. 1-5. Zurich: IEEE.

Winters, J. M. and Stark, L. (1988). Estimated mechanical properties of synergistic muscles involved in movements of a variety of human joints. *J. Biomech.* **21**, 1027-1041.

Zajac, F. E. and Gordon, M. E. (1989). Determining muscle's force and action in multi-articular movement. *Exerc. Sport Sci. Rev.* **17**, 187-230.

Zajac, F. E., Neptune, R. R. and Kautz, S. A. (2003). Biomechanics and muscle coordination of human walking: part II: lessons from dynamical simulations and clinical implications. *Gait Posture* **17**, 1-17.

The Journal of Experimental Biology

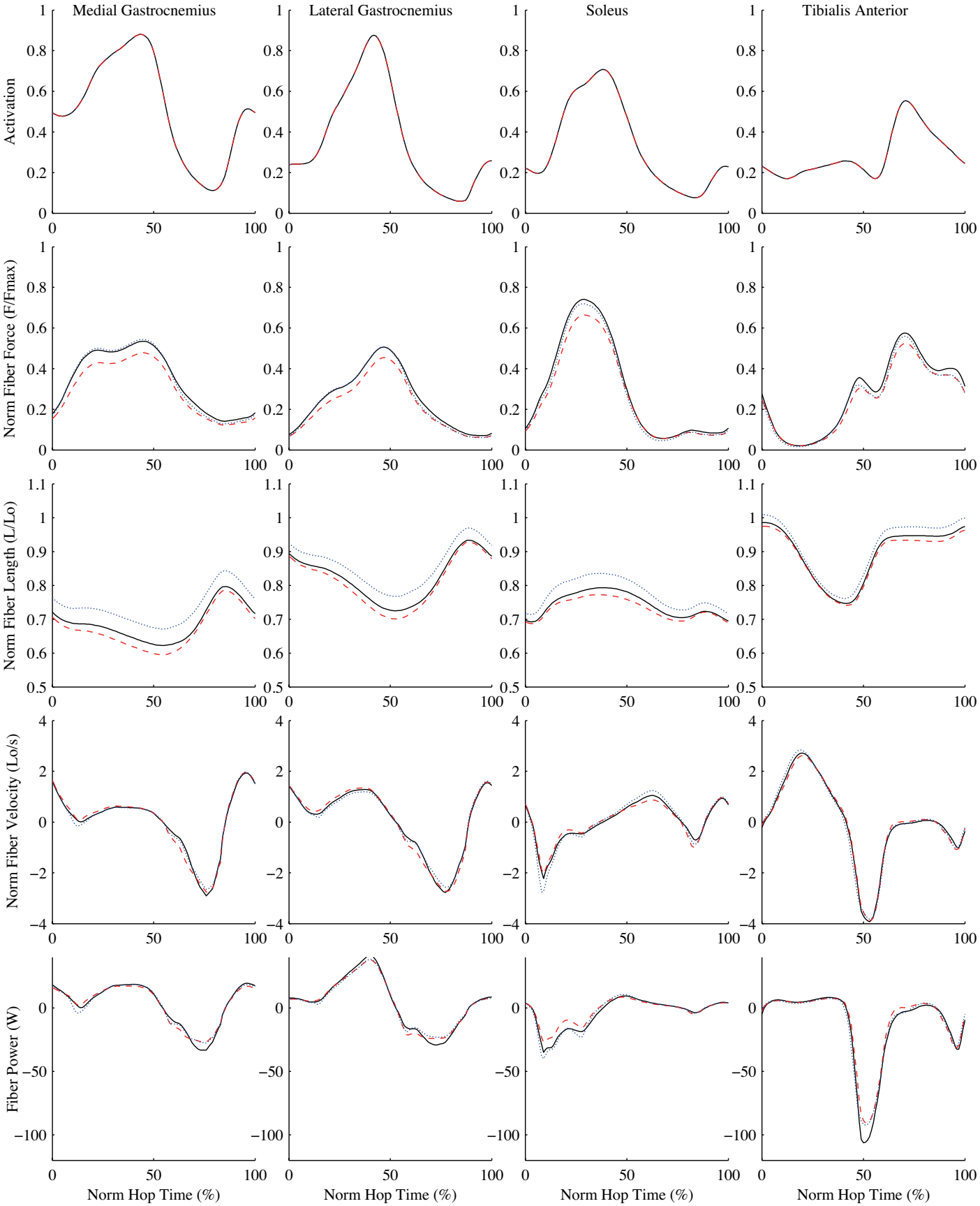

Fig. S1. Sensitivity of muscle dynamics to tendon compliance. The original simulations (black solid line) were recomputed with tendon compliance of all simulated muscles set ten percent greater (red dashed line) or ten percent less (blue dotted line) for one of the scaled musculoskeletal models.

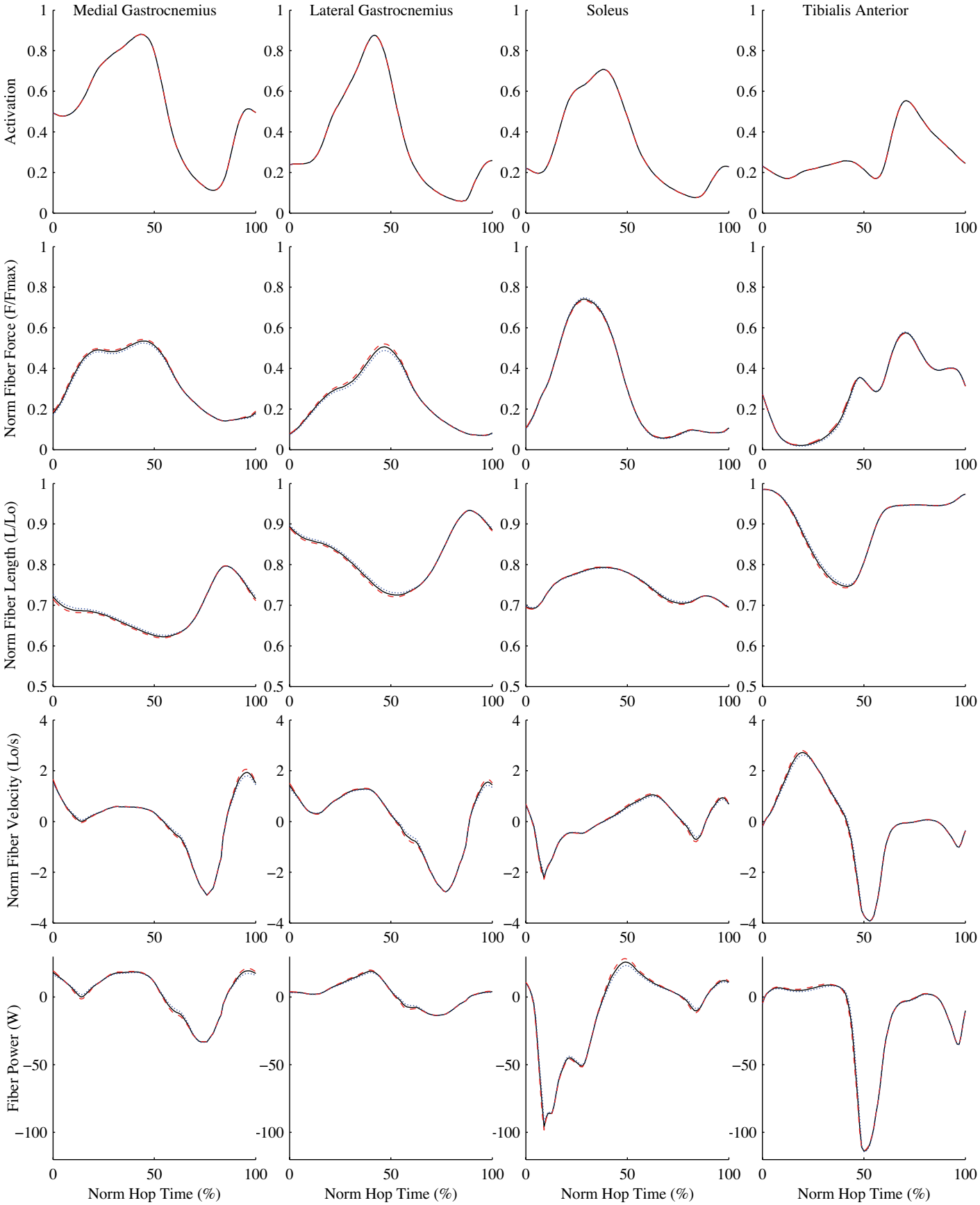

Fig. S2. Sensitivity of muscle dynamics to v_{max}. The original simulations (black solid line) were recomputed with v_{max} of all simulated muscles set ten percent greater (red dashed line) or ten percent less (blue dotted line) for one of the scaled musculoskeletal models.

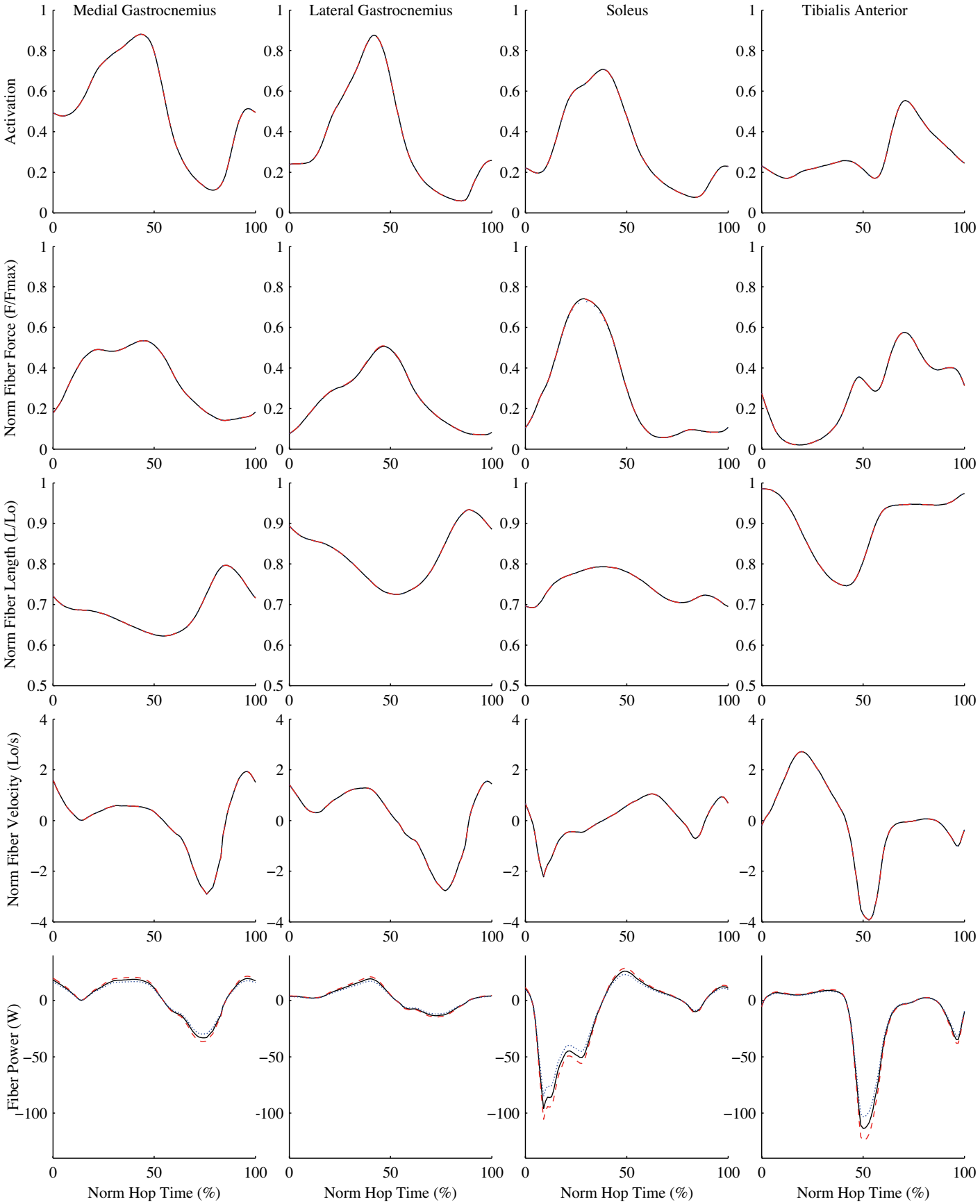

Fig. S3. Sensitivity of muscle dynamics to maximum isometric force (F_{max}). The original simulations (black solid line) were recomputed with F_{max} of all simulated muscles set ten percent greater (red dashed line) or ten percent less (blue dotted line) for one of the scaled musculoskeletal models.

Table S1. Sensitivity of metabolic energy consumption to muscle parameter values. Data are rate of metabolic energy consumption ($J \cdot kg^{-1} \cdot hop^{-1}$) for simulations using one scaled model where tendon stiffness, muscle maximum isometric force (F_{max}) and maximum shortening velocity (v_{max}) for all muscles were varied by ± 10% from those shown in Table 1

	Tendon Stiffness			**F_{max}**			**v_{max}**		
	- 10%	-	+10%	- 10%	-	+10%	- 10%	-	+10%
MG	0.176	0.164	0.155	0.150	0.164	0.178	0.166	0.164	0.162
LG	0.078	0.078	0.076	0.071	0.078	0.083	0.078	0.078	0.078
SO	0.170	0.172	0.203	0.148	0.172	0.196	0.171	0.172	0.172
TA	0.017	0.011	0.031	0.010	0.011	0.023	0.011	0.011	0.010
TOTAL	0.441	0.425	0.465	0.379	0.425	0.48	0.426	0.425	0.422